

13th U. S. National Combustion Meeting
Organized by the Central States Section of the Combustion Institute
March 19–22, 2022
College Station, Texas

Extinction of the Stagnation Point Diffusion Flame: Effect of Conductive Heat Loss into Solid Interior

Chengyao Li^{1,}, James T'ien¹, Michael Johnston²*

¹*Department of Mechanical and Aerospace Engineering, Case Western Reserve University, Cleveland, OH, USA*

²*NASA Glenn Research Center, Cleveland, OH, USA*

**Corresponding Author Email: chengyao.li@case.edu*

Abstract: The oxygen-versus-flow-velocity flammability boundary of a solid is U-shaped. The left side of the flammability boundary is the quenching branch, and the right side is the blow-off branch. Quenching is due to a weak flame whose heat release from combustion cannot overcome the excessive heat losses from, for example, radiation. Blow-off is due to a short gas residence time that is smaller than the chemical reaction time (traditionally referred to as the small Damköhler number effect). For thick solids, the heat conduction into the solid interior has a long transient after ignition before the solid temperature reaches the steady state. During this slow transient, there is excessive (i.e., more than that at the steady state) gas phase heat conduction into the solid interior. From the viewpoint of the quasi-static gaseous flame, this is an additional heat loss that will affect the gas flame's flammability.

In this work, a previously developed one-dimensional axisymmetric stagnation-point diffusion flame model is extended to account for the excessive heat loss into the solid beyond the steady burning state. A non-dimensional excessive conductive heat loss parameter Ψ is defined in the paper to account for the transient solid effect. For each Ψ , the gas phase is considered reaching a quasi-steady state. Extensive numerical computations have been performed to determine the extinction boundary and the characteristics of near-limit flames. The U-shaped flammability boundary is now a series of boundaries with Ψ as a parameter.

Flame structures under the same environment condition but with different Ψ are compared. For a given oxygen ambient, the extinction boundary of Ψ versus stretch rate is an inverted U-shape. The boundary consists of a blowoff branch and a radiative quenching branch. Extensive computed data including flame and pyrolysis temperatures, burning rate, flame standoff distance, species concentration, and reaction rate are presented along the extinction boundaries. Heat balance analysis is performed for both the gas phase and the gas-solid interface. Along the extinction boundary, the relative importance of conduction, convection, radiation, and chemical reaction are analyzed in detail.

Keywords: *Stagnation-point diffusion flame, Material flammability, Excessive conductive heat loss, Extinction boundary*

1. Introduction

The flammability boundary of a solid is U-shaped. The left side of the flammability boundary is the quenching branch, and the right side is the blow-off branch. Quenching is due to a weak flame whose heat release from combustion cannot overcome the excessive heat losses from, for example, radiation [1]. Blow-off is due to a short gas residence time that is smaller than the chemical reaction time (traditionally referred to as the small Damköhler number effect, e.g., [2]).

There are extensive studies on solid flammability boundary in recent decades [3-9]. The ordinate can be ambient oxygen percentage or total pressure and the abscissa represents flow velocity, gravity level, stretch rate, etc.

Consider the illustration of a general temperature profile at the gas-solid interface of a burning thick solid as shown in Fig. 1. The heat input from flame to the solid through radiation and convection is used to decompose the solid material to fuel vapors, to transfer heat to the ambient through solid surface radiation, and to heat up the solid interior through heat conduction. To the gas flame, the solid heat conduction is a loss. This conductive heat loss decreases with time in the solid transient until the solid temperature profile reaches steady state. With larger heat losses, the mass burning rate is smaller and the flame is weaker. When the mass burning rate is below a certain value (magnitude may depend on fuel and environment), the flame becomes un-sustained [10, 11].

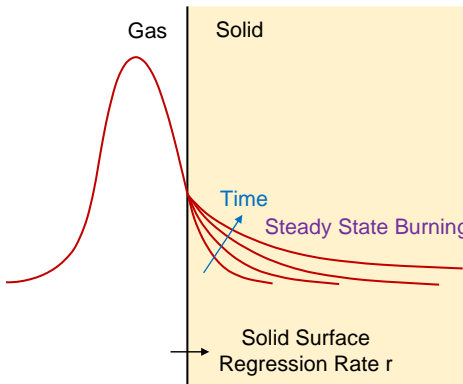


Figure 1: Illustration of gas-solid-interface temperature profile after ignition

In T'ien et al.'s modeling work of the stagnation flame over thick polymethyl methacrylate (PMMA), the solid phase is considered reaching steady state of the convection-conduction balance (convection is due to the movement of the regression surface in a coordinate attached to the burning surface) [1, 12]. From dimension analysis, the time scale for a thick solid to reach the steady convection-conduction balance is of the order α_s/r^2 , where α_s is the thermal diffusivity of the solid and r is the surface regression rate due to combustion. Since the solid burning rate is typically very small, the time scale for reaching the steady state can be very long (of the order of many minutes). In other word, the burning of a thick solid may be mostly in a transient solid state although the gas-phase can be considered to be quasi-steady.

There are some early works investigating the material flammability beyond the steady solid phase description. Yang and T'ien developed a two-dimensional numerical model for flame over a PMMA cylinder in a cross flow [13]. The model has a quasi-steady gas-phase and a simplified solid phase. Flame radiation was neglected. The percentage of conductive heat flux into the solid out of the convective heat flux from the gas phase Φ was treated as an input parameter. Above a critical Φ , no flame exists for any flow rate. Below a critical Φ , a low-speed quenching boundary exists but there are two blowoff boundaries in higher flow speeds. Beyond the first boundary, flame blows off at the forward stagnation point of the cylinder and the envelope flame transitioned to a wake flame. The wake flame blows off at a much higher flow velocity. Experimentally, Goldmeer et al. used parabolic flight to reach low-gravity conditions to examine the low-pressure extinction boundary of the diffusion flame over PMMA cylinders (diameter of 1.9 cm) [14]. The solid center temperature was measured and serves as an indicator of the degree of heating. Results showed that at higher solid center temperature, the extinction pressure is lower. The model from Yang and T'ien [13] was extended to include a transient description of the solid heat transfer. Good agreement between experiment and simulation was achieved. Wu et al. experimentally investigated the extinction of

PMMA sphere in a semi-quiescent microgravity environment using a 3.6-s drop tower [15]. A stable flame is established in normal gravity before the transient to microgravity. The effect of fuel curvature, solid surface radiation, and solid-phase heat conduction on flame extinction was studied. It was observed that, as the burning duration increases, the flame extinction in microgravity is delayed or prevented due to less conductive cooling.

To further our understanding and to systematically quantify the material flammability in terms of the solid preheating level and the environmental parameters (ambient pressure, oxygen percentage, and incoming flow speed), a microgravity fire project Growth and Extinction Limit (GEL) is designed and will be performed in the Combustion Integrated Rack (CIR) aboard the International Space Station (ISS). The test samples are 4-cm-diameter custom cast PMMA spheres with five imbedded thermocouples. The conductive heat loss into the solid interior can be reconstructed using thermocouple measurements. In the past few years, precursor but stand-alone studies have been conducted to support the GEL project. Endo et al. developed a detailed transient two-dimensional numerical model to study the effect of solid in-depth heat-up on flame growth [16]. Li et al. studied the ignition of PMMA sphere using hot wire igniter [17]. Johnston et al. studied the dynamic response and induced quenching extinction in normal to zero gravity transition for PMMA sphere [18]. Two parameters were investigated: the forced flow velocity and the degree of preheating in the surface layer of the GEL sample. A flammability map in terms of conductive heat flux at the stagnation point versus stretch rate is established at 17% oxygen.

There is a need of systematic study of flammability boundary with the quantification of the internal temperature gradient of a thick solid. In this work, previously developed one-dimensional axisymmetric stagnation-point diffusion flame model by T'ien [1] is extended to account for the excessive heat loss into the solid beyond the steady burning state. The excessive conductive heat loss, together with oxygen mass fraction and the stretch rate are systematically varied to study the extinction of the stagnation point diffusion flame.

2. Numerical Model

The numerical model in this work is extended from a previously developed one-dimensional axisymmetric steady stagnation-point diffusion flame model [1]. As discussed in the introduction section, the solid-phase time scale is much longer than the gas-phase. The gas phase is considered reaching quasi-steady state for each time instance of the solid phase. Similar approaches were also considered by Endo et al. [16] and Yang and T'ien [13] to save computational time. The gas-phase conservation equations are similar to T'ien et al.'s work [1, 12] but are summarized below for completeness.

$$\text{Continuity} \quad \frac{1}{r^\epsilon} \frac{\partial(r^\epsilon \rho u)}{\partial r} + \frac{\partial(\rho v)}{\partial y} = 0 \quad (1)$$

$$\text{Momentum} \quad \rho \left(u \frac{\partial u}{\partial r} + v \frac{\partial u}{\partial y} \right) = - \frac{\delta p}{\delta r} + \frac{\partial}{\partial y} \left(\mu \frac{\partial u}{\partial y} \right) \quad (2)$$

$$\text{Energy} \quad \rho u c_p \frac{\partial T}{\partial r} + \rho v c_p \frac{\partial T}{\partial y} = \frac{\partial}{\partial y} \left(\frac{\lambda}{c_p} \frac{\partial T}{\partial y} \right) - \frac{\partial}{\partial y} q_r'' + qw \quad (3)$$

$$\text{Species} \quad \rho u \frac{\partial Y_i}{\partial r} + \rho v \frac{\partial Y_i}{\partial y} = \frac{\partial}{\partial y} \left(\rho D \frac{\partial Y_i}{\partial y} \right) + N_i w \quad (4)$$

The Arrhenius law for the gas-phase fuel reaction rate is $w = W_F(B^*T)\rho^2 \frac{Y_F}{W_F} \frac{Y_O}{W_O} \exp(-\frac{E}{RT}) = \rho B Y_F Y_O \exp(-\frac{E}{RT})$.

In T'ien's work, gas-phase radiation is neglected but the solid surface radiation loss is considered in the solid surface energy balance [1]. Though simplified, T'ien's work leads to the

successful identification of the radiative quenching limit. In this work, an efficient but robust corrected Planck mean absorption approximation is used together with the two-flux model in solving the gas-phase radiative transfer equation [4, 19, 20]. The gas phase is considered non-scattering gray media with CO₂ and H₂O the participating medium.

$$\text{Two-flux model} \quad \begin{cases} \frac{1}{2K} \frac{dq^+}{dy} + q^+ = q_b \\ -\frac{1}{2K} \frac{dq^-}{dy} + q^- = q_b \end{cases} \quad (5)$$

The radiative heat flux vector in Eq. (3) is expressed as $q''_r = q^+ - q^-$. K , the absorption coefficient is the Planck mean absorption coefficient multiplied by a correction factor that is an empirical function of the “pseudo optical length”, $\int_0^\infty \kappa_p dy$. It follows Rhatigan’ work [4]. The Planck mean absorption coefficients for participating media are piecewise polynomial functions of the local temperature following Tien’s work [20] that will not repeat here. The local Planck mean absorption coefficients κ_p is calculated as the summation of the partial pressure weighted values of the Planck mean absorption coefficients of the participating species. The boundary conditions for the radiation model are:

$$\begin{cases} q^+ = \varepsilon_s \sigma T_s^4 + (1 - \alpha_s) q^- & y = 0 \\ q^- = \sigma T_e^4 & y = \infty \end{cases} \quad (6)$$

The boundary conditions for other gas-phase conservation equations at the far ambient are:

$$\begin{cases} T = T_e \\ u = u_e = ar \\ Y_F = 0 \\ Y_O = Y_{O,e} \end{cases} \quad (7)$$

a is the stretch rate at the stagnation point. At the solid surface, non-slip condition is assumed ($u = 0$). Instead of solving the transient solid conservation equations, the solid surface temperature is directly solved from the energy balance:

$$\lambda_g \frac{\partial T}{\partial y} \Big|_g = (1 + \Psi) \bar{m}'' c_s (\bar{T}_s - T_c) + \dot{m}'' L + q''_{r,s} \quad (8)$$

Bars in Eq. (8) denotes the steady-state solution of the following:

$$\lambda_g \frac{\partial \bar{T}}{\partial y} \Big|_g = \bar{m}'' [c_s (\bar{T}_s - T_c) + L] + \bar{q}_{r,s}'' \quad (9)$$

where the convection term due to surface regression $\bar{m}'' c_s (\bar{T}_s - T_c)$ is balanced by the solid-phase heat conduction $\lambda_s \frac{\partial \bar{T}}{\partial y} \Big|_s$. The mass burning rate is related to the solid surface temperature following the Arrhenius law: $\dot{m}'' = b \exp\left(\frac{-E_s}{RT_s}\right)$. The latent heat is evaluated from $L = L_0 + (c_p - c_s)T_s$. The solid surface radiative heat flux is solved from the two-flux radiative model with $q''_{r,s} = (q^+ - q^-)_{y=0}$. In Eq. (8), Ψ is the dimensionless excessive conductive heat loss $\Psi =$

$\left(\lambda_s \frac{\partial T}{\partial y} \Big|_s - \lambda_s \frac{\partial \bar{T}}{\partial y} \Big|_s\right) / \lambda_s \frac{\partial \bar{T}}{\partial y} \Big|_s$. In other word, Eq. (8) solves the transient state beyond the steady state for each given Ψ . Numerically, Eq. (9) together with the gas-phase conservation equations are first solved. Then \bar{T}_s and Ψ are used as inputs to solve solid surface temperature in Eq. (8).

The march-in-time technique is used to obtain the steady-state solutions by adding a fictitious unsteady term to the conservation equations as detailed in [12]. Except the species equations for Y_F and Y_O (Eq. (3)) are treated implicitly, all other unsteady terms use the explicit scheme. Upwind scheme is used for convection terms. The partial differential equations are solved with the finite difference method.

Table 1: Property values

Property	Physical meaning	Value
p_e	ambient pressure	1atm
T_e	ambient temperature	300K
T_c	temperature deep inside the solid	300K
ρ_e	ambient density	1.177 kg/m^3
λ_e	ambient thermal conductivity	$2.638 \times 10^{-2} \text{ W/m/K}$
μ_e	ambient dynamic viscosity	$1.845 \times 10^{-5} \text{ kg/m/s}$
σ	Stefan-Boltzmann constant	$5.6704 \times 10^{-8} \text{ W/m}^2/\text{K}^4$
B	pre-exponential factor for gas-phase chemical reaction	$5.047 \times 10^7 \text{ s}^{-1}$
b	pre-exponential factor for solid-phase pyrolysis	$2.32 \times 10^7 \text{ kg/m}^2/\text{s}$
ϵ	0 for two-dimensional flow; 1 for axisymmetric flow	1 (axisymmetric)
E	activation energy for gas-phase chemical reaction	$1.13 \times 10^5 \text{ J/mol}$
E_s	Activation energy for solid-phase pyrolysis	$1.25 \times 10^5 \text{ J/mol}$
q	heat of combustion	$2.07 \times 10^7 \text{ kJ/kg}$
L_0	latent heat at 0 K	$8.37 \times 10^5 \text{ kJ/kg}$
Pr	Prandtl number	0.7
Sc	Schmidt number	0.7
c_s/c_p	solid-phase specific heat / gas-phase specific heat	1.17
ε_s	solid surface radiation emissivity	0.9
α_s	solid surface radiation absorptivity	0.9

Property values used in this work are summarized in Table 1. The diffusion coefficients and specific heats of different species are assumed to be equal and constant. Prandtl and Schmidt numbers are also constants. Ideal gas law is assumed for the mixture and each component gas. The product of local density and viscosity is assumed constant across the computational domain.

All the equations are solved in their nondimensional forms. Nondimensionalization is similar to T'ien et al.'s work [1, 12]. Uniform 500 grids are distributed along 5 nondimensional length. In the following simulations, the dimensionless excessive conductive heat loss, oxygen mass fraction, and the stretch rate are systematically varied across the whole flammability range.

3. Results and discussions

An example of the comparison of the flame structures between the steady-state and near-extinction flames is shown in Fig. 2. In a 7.5 s^{-1} stretch rate air flow, flame is steady when the solid conduction-convection balance is reached. In a transient state, when the dimensionless excessive conductive heat loss is larger than 1.58, the flame cannot sustain itself, or in other word, go through extinction. Due to increased heat loss into the solid, the flame enhances its heat input to the solid

from convective heat transfer to maintain a critical mass burning rate. It is through a shorter flame standoff distance and hence steeper temperature gradient at the solid surface. The fuel fraction at the solid surface is also smaller because of the reduced mass burning rate. As a result of the additional heat loss, the gas-phase reaction rate and flame temperature both decreases. Though a global one-step second-order kinetics is used for the gas phase, the computation reveals the classical near-extinction flame structure. At the flame standoff distance, there is slightly more fuel and oxygen leftover compared with the steady case. One may also notice the flame is fatter when near extinction.

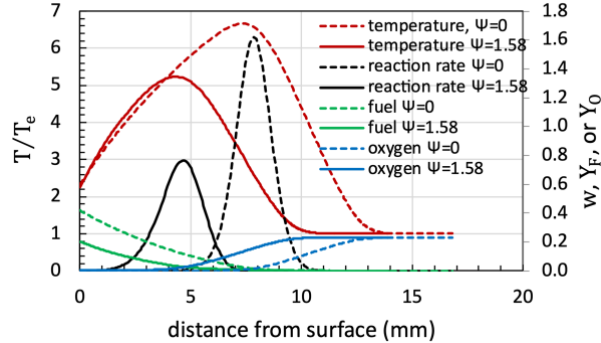


Figure 2: Flame structures at steady state ($\Psi = 0$) and near extinction ($\Psi = 1.58$) for the same ambient condition: $a = 7.5\text{s}^{-1}$, $Y_{O_2} = 23.1\%$

The same computation can be easily extended to variable stretch rate and oxygen concentration. Figure 3 shows the extinction boundaries of dimensionless excessive conductive heat loss versus stretch rate. They have an inverted U-shape with the left quenching branch and right blow-off branch. The abscissa is the steady state solutions. Further away from the upper and lower stretch rate limits, the flame is more sustained with larger heat loss. The turning point from the quenching branch to the blowoff branch (maximum Ψ) is at 7.5s^{-1} , for example, with 23.1% ambient oxygen, with detailed flame structure shown in Fig. 2. The maximum Ψ is higher at larger oxygen concentration. It also occurs at slightly larger stretch rate with the increase of oxygen mass fraction.

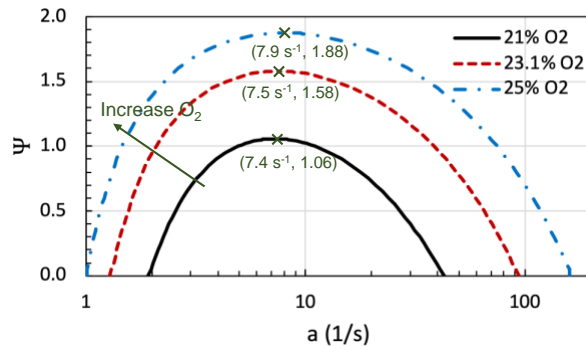


Figure 3: Extinction boundary of dimensionless excessive conductive heat loss versus stretch rate at various oxygen concentrations

Selecting air as an example, the flame profiles are also plotted along the extinction boundary in Fig. 4. For both plots, the quenching branch is on the left and the blowoff branch is on the right. With the increase of stretch rate from left to right, maximum gas-phase reaction rate and maximum

flame temperature both increases. From the example case in Fig. 2, one observes that the two peaks are not at the same location. Another result of increased stretch rate (oxidizer flow rate) is decreased flame standoff distance. The combined effect of increased flame temperature and decreased flame standoff distance is increased convective heat transfer from the flame to the solid surface, increased mass burning rate, and slightly increased solid surface temperature. The fuel and oxygen mass fractions are also plotted at the maximum reaction rates. From quenching to blowoff, the oxygen mass fraction slightly increases, and the fuel mass fraction significantly increases. On the blowoff branch, there are more fuel vapor is left over and carried away to sides by convection flow. Note the flame standoff distance follows around the cube root power law as predicted by rod stagnation point flame experiments by Olson and Ferkul [21].

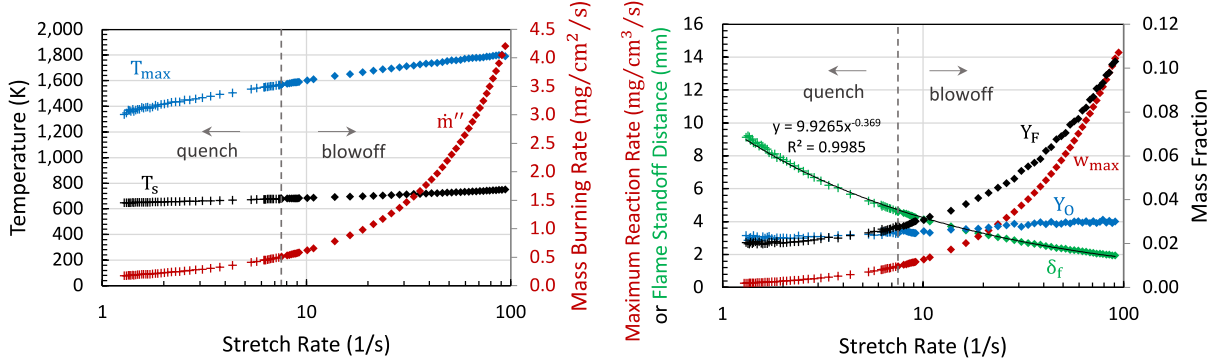


Figure 4: Flame profiles along the Ψ -a extinction boundary. Left: gas and solid surface profiles; Right: profiles at the maximum reaction rates. ($Y_{O_2} = 23.1\%$)

To evaluate the energy balance along the extinction boundary, two practices are taken. We first consider the gas-phase energy conservation in Fig. 5 and then the control-volume heat transfer analysis in Fig. 6.

For the gas-phase energy conservation equation, the following dimensionless form provides more insights.

$$\frac{1}{Pr} \theta'' + f \theta' - \frac{4}{1+\epsilon} \frac{SD_k}{Pr} \left(\theta^4 - \frac{\hat{q}^+ + \hat{q}^-}{2} \right) = \hat{q} \hat{w} \quad (10)$$

Hats in Eq. (10) denotes dimensionless variables to be different from their dimensional forms. The heat of combustion is nondimensionalized by $c_p T_e$. The radiative heat flux is nondimensionalized by σT_e^4 . The dimensionless temperature θ is T/T_e . The dimensionless reaction rate is related to w by $\hat{w} = \frac{1+\epsilon}{2} \rho a w$. f is the modified stream function that is related to the axial velocity by $\frac{u}{u_e} = \frac{1}{2} f \eta$ and η is the dimensionless length. S and D_k are nondimensional radiation parameters as defined in [22]. Equation (10) can then be identified constituting of four parts: conduction, convection, radiation, and generation of heat. They are then plotted separately in Fig. 5. Stretch rates range from quenching to blowoff in Fig. 5. The peak of dimensionless heat generation (or peak of dimensionless reaction rate) is almost invariant. The dimensionless width of reaction zone is also almost invariant ($\sim 0.5\eta$). Considering $\frac{dy}{d\eta} = \sqrt{Sc \frac{D}{a}}$, the dimensional reaction width scales up with diffusion distance. In the reaction zone, heat generation is mainly balanced by conduction. Heat convection kicks in from the middle of the reaction zone and above. It takes away the heat conducted upstream of the reaction zone. From quenching to blowoff in Fig. 5, the relative

importance of gas-phase radiation loss decreases but that of heat convection to sides increases as expected.

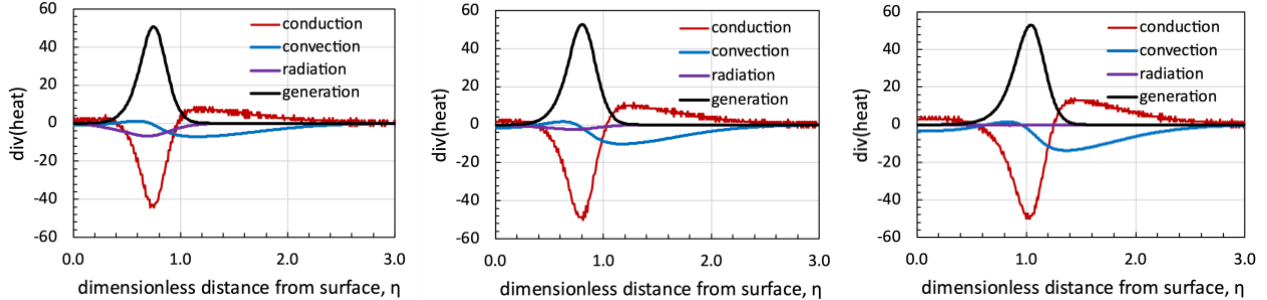


Figure 5: Gas-phase energy conservation at three selected stretch rates along the Ψ - a extinction boundary. Left: $a = 1.28 \text{ s}^{-1}$; Middle: $a = 7.5 \text{ s}^{-1}$; Right: 94.29 s^{-1} . ($Y_{O_2} = 23.1\%$)

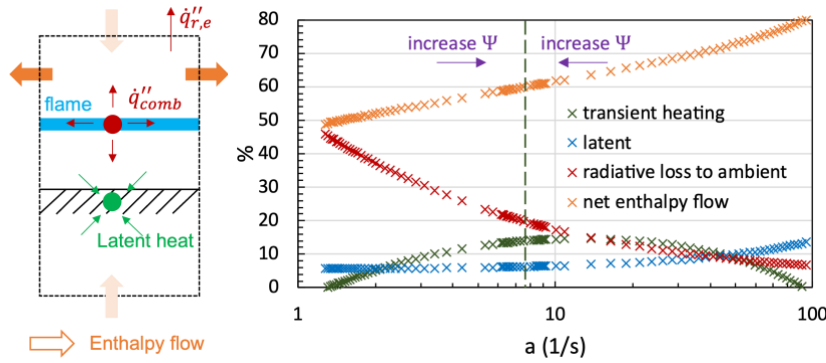


Figure 6: Heat transfer analysis along the Ψ - a extinction boundary. Left: schematic of the control volume and the heat balance; Right: heat terms nondimensionalized by the combustion heat \dot{q}_{comb}'' versus stretch rates. ($Y_{O_2} = 23.1\%$)

Now we consider the control volume in Fig. 6 that covers from deep inside the solid to the far ambient oxidizer flow. In this work, they are assumed at the same ambient temperature 300 K. Fixing the origin at the solid surface stagnation point, the solid surface regression can be seen as virgin fuel feeding at the far ambient boundary with the same regression rate. In other word, there are virgin fuel and fresh oxidizer enthalpy flow feeding into the control volume at 300 K. There is also hot enthalpy flow to two sides carrying combustion products and some fuel vapor and oxygen leftover. These are the mass flow crossing the boundaries of the control volume. Inside the control volume, the combustion heat from chemical reactions is the heat source and the latent heat used for solid decomposition is a heat sink. An additional heat transfer across the boundary is the radiative heat loss to the ambient. The energy conservation of the control volume can then be simply summarized as: combustion heat = latent heat + enthalpy flow + radiative loss + transient heating of the solid. The transient heating of the solid is the time derivative of temperature term. It represents the excessive heat used to heat up the solid before the steady state. Nondimensionalizing each term by the combustion heat, they are plotted against stretch rate along the extinction boundary in the right of Fig. 6. With the increase of stretch rate, the radiative loss decreases and the net enthalpy flow to two sides increases as discussed in Fig. 5. There is also expected latent heat increasing with stretch rate because the mass burning rate increases along the extinction boundary as shown in Fig. 4. On the quenching branch, radiation loss is significant. It takes as much as 46% of the total combustion heat generation. On the blowoff branch, gas residence time is too short compared with chemical reaction time. There is also more heat taken away with the convective flow with a

maximum of 80%. In the middle of the extinction boundary, flame can survive with excessive heat loss. In the configuration of this work, it is the heat conduction into the solid interior. The transient heating “loss” can be up to 15%.

Switching Ψ and oxygen mass fraction in plotting the extinction boundary in Fig. 3, one can achieve the classic U-shape flammability boundary in Fig. 7. It now becomes a function of Ψ , the dimensionless excessive conductive heat loss. It is an additional parameter that affects the material flammability boundary of thick solid but has attracted less attentions in the past. As demonstrated in the introduction section, the transient state before the steady state can be in the order of many minutes and hence dominates the whole experiment process.

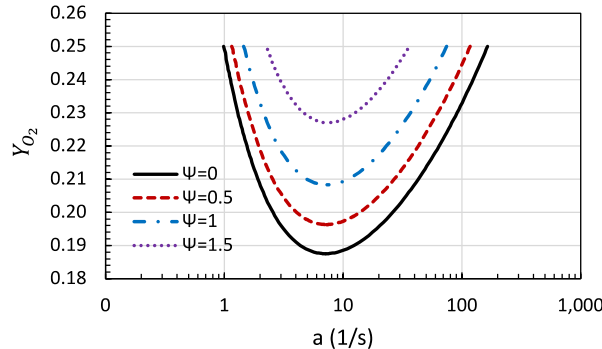


Figure 7: U-shape oxygen-versus-stretch-rate flammability boundaries as function of dimensionless excessive conductive heat losses

4. Conclusions

A previously developed one-dimensional axisymmetric stagnation-point diffusion flame model is expanded to account for the excessive conductive heat loss into thick solid beyond the steady burning state. A non-dimensional excessive conductive heat loss parameter Ψ is defined. Extensive numerical computations have been performed to determine the extinction boundary and the characteristics of near-limit flames.

The classical U-shaped flammability boundary in the oxygen vs. stretch rate plot now becomes a series of U-shaped boundaries as a function of Ψ . For a given oxygen ambient, the extinction boundary of Ψ versus stretch rate is an inverted U-shape. It consists of a radiative quenching branch and a blowoff branch. Extensive computed data including flame and pyrolysis temperatures, burning rate, flame standoff distance, species concentration, and reaction rate are presented to compare the near-limit flame structures along the extinction boundary. Energy balance analysis along the extinction boundary is also practiced to identify individual contributions of energy terms.

5. Acknowledgements

This work was supported by NASA (grant number NNX16AE84A). We would like to thank Dr. Paul Ferkul and Dr. Sandra Olson for their constant consultations.

6. References

- [1] J.S. T’ien, Diffusion flame extinction at small stretch rates: the mechanism of radiative loss, Combust. Flame 65 (1986) 31-34.

- [2] F.E. Fendell, Ignition and extinction in combustion of initially unmixed reactants, *J. Fluid Mech.* 21 (1965) 281-303.
- [3] D.W. Fouch, J.S. T'ien, Extinction of a stagnation point diffusion flame at reduced gravity, *AIAA J.* 25 (1987) 972-976.
- [4] J.L. Rhatigan, H. Bedir, J.S. T'ien, Gas-phase radiative effects on the burning and extinction of a solid fuel, *Combust. Flame* 112 (1998) 231-241.
- [5] A. Kumar, J.S. T'ien, A computational study of low oxygen flammability limit for thick solid slabs, *Combust. Flame* 146 (2006) 366-378.
- [6] S.-Y. Hsu, J.S. T'ien, Pressure extinction limits of non-premixed flames, *Combust. Theory Model.* 13 (2009) 885-900.
- [7] F. Zhu, Z. Lu, S. Wang, Flame spread and extinction over a thick solid fuel in low-velocity opposed and concurrent flows, *Microgravity Sci. Technol.* 28 (2016) 87-94.
- [8] J.W. Marcum, P.V. Ferkul, S.L. Olson, PMMA rod stagnation region flame blowoff limits at various radii, oxygen concentrations, and mixed stretch rates, *Proc. Combust. Inst.* 37 (2019) 4001-4008.
- [9] A.V. Ivanov, Y.V. Balashov, T.V. Andreeva, A.S. Melikhov, Experimental verification of material flammability in space, NASA CR-1999-209405, NASA Glenn Research Center, Cleveland, OH 1999.
- [10] D. Rich, C. Lautenberger, J.L. Torero, J.G. Quintiere, C. Fernandez-Pello, Mass flux of combustible solids at piloted ignition, *Proc. Combust. Inst.* 31 (2007) 2653-2660.
- [11] M.C. Johnston, J.S. T'ien, Gravimetric measurement of solid and liquid fuel burning rate near and at the low oxygen extinction limit, *Fire Saf. J.* 91 (2017) 140-146.
- [12] J.S. T'ien, S. Singhal, D.P. Harrold, J.M. Prahl, Combustion and Extinction in the Stagnation-Point of a Condensed Fuel, *Combust. Flame* 33 (1978) 55-68.
- [13] C.T. Yang, J.S. T'ien, Numerical simulation of combustion and extinction of a solid cylinder in low-speed cross flow, *J. Heat Transfer*, 120 (1998) 1055-1063.
- [14] J.S. Goldmeer, J.S. T'ien, D.L. Urban, Combustion and extinction of PMMA cylinders during depressurization in low-gravity, *Fire Saf. J.* 32, 61-88 (1999).
- [15] C. Wu, P. Sun, X. Wang, X. Huang, S. Wang, Flame extinction of spherical PMMA in microgravity: effect of fuel diameter and conduction, *Microgravity Sci. Technol.* 32 (2020) 1065-1075.
- [16] M. Endo, J.S. T'ien, P.V. Ferkul, S.L. Olson, M.C. Johnston, Flame growth around a spherical solid fuel in low speed forced flow in microgravity, *Fire Technol.* 56 (2020) 5–32.
- [17] C. Li, J.S. T'ien, M.C. Johnston, S.L. Olson, P.V. Ferkul, Ignition of thermally-thick blunt body PMMA samples using a heated wire, *Fire Saf. J.* 133 (2022) 103663.
- [18] M.C. Johnston, J.S. T'ien, S.-Y. Hsu, C.-W. Wu, S.L. Olson, P.V. Ferkul, Dynamic response and induced quenching extinction of solid sphere diffusion flames in normal to zero gravity transition: effect of sample subsurface pre-heating, *Combust. Flame* (under review).
- [19] J.B. Armstrong, S.L. Olson, J.S. T'ien, Transient model and experimental validation of low-stretch solid-fuel flame extinction and stabilization in response to a step change in gravity, *Combust. Flame* 147 (2006) 262-277.
- [20] C.L. Tien, Thermal Radiation Properties of Gases, in: T.F. Irvine, J.P. Hartnett (Eds), *Advances in Heat Transfer*, Academic Press, New York, 1968, vol. 5, pp. 234-254.
- [21] S.L. Olson, P.V. Ferkul, Microgravity flammability boundary for PMMA rods in axial stagnation flow: experimental results and energy balance analyses, *Combust. Flame* 180 (2017) 217-229.
- [22] J.L. Rhatigan, Effects of gas-phase radiation and detailed kinetics on the burning and extinction of a solid fuel, Ph.D. thesis, Case Western Reserve University, 2001.